J. Opt. A: Pure Appl. Opt. **11** (2009) 045705 (9pp) doi:10.1088/1464-4258/11/4/045705

# Blaze produced by a dual-period array of subwavelength cylinders

**Marcelo Lester**[1,3], **Diana C Skigin**[2,3] **and Ricardo A Depine**[2,3]

[1] Instituto de Física Arroyo Seco, Facultad de Ciencias Exactas, Universidad Nacional del Centro de la Provincia de Buenos Aires, Pinto 399 (cp 7000) Buenos Aires, Argentina
[2] Grupo de Electromagnetismo Aplicado, Departamento de Física, Facultad de Ciencias Exactas y Naturales, Universidad de Buenos Aires, Ciudad Universitaria, Pabellón I, C1428EHA Buenos Aires, Argentina

E-mail: mlester@exa.unicen.edu.ar, dcs@df.uba.ar and rdep@df.uba.ar

Received 12 August 2008, accepted for publication 22 December 2008
Published 16 January 2009
Online at stacks.iop.org/JOptA/11/045705

**Abstract**
We propose an alternative way of enhancing the intensity diffracted by a grating in a given direction using a dual-period array. Each period comprises several identical cylinders with diameters much smaller than the incident wavelength (subwavelength cylinders), whose axes are aligned in a plane which is tilted with respect to the periodicity direction. We present results for metallic and dielectric cylinders, and show that in both cases this structure behaves like a blazed grating in the sense of its capability to enhance the intensity in a pre-designed direction. This blazed-like behavior is found for both incident polarization modes. If we consider the quick evolution of manufacturing techniques of nanogratings, such structures constitute a realizable alternative not only for the microwave and millimeter wave regions but also for optical devices.

**Keywords:** dual-period gratings, blaze, diffraction

(Some figures in this article are in colour only in the electronic version)

## 1. Introduction

Dual-period infinite gratings—in which each period is formed by a subarray of cylinders forming a finite grating—have not received much attention until recently. These structures offer more versatility for the design of optical devices than the usual gratings, since they have more geometrical parameters that can be controlled to make them adequate for a particular purpose. The dual-period characteristic of gratings has been recently studied in connection with the coupling of surface plasmon polaritons to the incident wave [1–3] to control simultaneously the modes of a broad-area diode laser [4] and to design electromagnetic resonance enhanced silicon-on-insulator photodetectors [5–7]. Gratings with a period comprising slits and grooves have been shown to modify the transmission response [8], while infinite compound gratings have recently been shown to exhibit remarkable properties. In particular, they can support phase resonances which are characterized by a field enhancement within the cavities or slits, producing sharp features in the electromagnetic response. The effect of phase resonances on the response of reflection gratings was studied for gratings formed by rectangular grooves on a metallic substrate [9–13]. Later on, phase resonances were also found in transmission gratings comprising several subwavelength slits in each period [14–18].

It has been recently shown that blazed-binary diffractive optical elements composed of subwavelength patterns in a dielectric material have a remarkable performance in comparison with that achieved with a classical echelette grating [19–22]. Also, the use of high-index materials for the fabrication of subwavelength diffractive components operating in the visible domain has been reported [23]. Different design methods of blazed gratings consisting of a binary grating with subwavelength structures for a multilevel phase modulation have been proposed, taking into account the constraints in actual fabrication techniques [24]. In addition, etched blazed gratings have been shown to achieve high efficiencies in high orders; these results present opportunities for high-resolution EUV spectroscopy in astrophysics [25, 26], and blazed gratings with mounted deterministic subwavelength roughness have

[3] Member of CONICET.

 

been recently fabricated to optimize their properties [27]. In the search for more flexibility in generating arbitrary effective-index distributions in the direction of the grating period, novel ways have been proposed to design gratings with desired diffraction properties by using subwavelength feature sizes perpendicular to the ordinary superwavelength grating period [28]. Blazed-binary diffractive elements composed of pillars arranged on a two-dimensional grid have also been analyzed [29, 30].

Recent studies have shown that compound gratings made of cylinders can be designed to fulfill certain conditions such as the intensification or minimization of the intensity diffracted in a given order [31, 32]. These properties have been shown to be purely geometric effects, independent of the materials and cross section of the wires.

In this paper we enlarge the scope of compound structures and add a new degree of freedom to the structures considered in [32]: the array now consists of several equally spaced identical subarrays, each of them comprising a finite number of cylinders. All the cylinder axes in each subarray are contained in the same plane, which is inclined with respect to the periodicity direction. This is not a mere extension of the analysis made in [32], but instead the present configuration exhibits novel and interesting properties that lead to new possibilities for the design of diffractive structures. In particular, since these systems are reminiscent of echelette gratings commonly used to maximize the intensity in a non-specular direction, we study a similar blaze effect that can be achieved in such structures when the diameter of the cylinders is smaller than the incident wavelength (subwavelength cylinders).

The results shown are calculated using an integral method [33] that was implemented numerically to solve the scattering problem of a compound array of circular cylinders illuminated by a Gaussian beam. Metallic and dielectric constituents as well as both polarization modes of the incident beam are considered: s (electric field parallel to the cylinders' axes) and p (magnetic field parallel to the cylinders' axes).

In section 2 we describe the geometrical configuration, briefly discuss the integral method used for calculation of the field scattered by arrays of cylinders, and develop a simple scalar model to predict the response of compound structures. In section 3 we provide numerical results; we analyze the evolution of the reflected and transmitted intensity as a function of the inclination and the observation angle, and compare the results with those obtained by the scalar model. The dependence of the blaze effect on the geometrical parameters of the array is also studied. Concluding remarks are given in section 4.

## 2. Configuration and approach

The structure under study is a finite array of $N$ cylinders of radius $r$ and circular cross section in vacuum. The cylinders are grouped in $M$ subarrays, each of which comprises $J$ cylinders ($N = MJ$) whose axes are separated a distance $d$. In the scheme of figure 1 $N = 15$, $M = 3$ and $J = 5$. Although each subarray constitutes a finite grating (and not a periodic structure), we will designate the parameter $d$ as the period

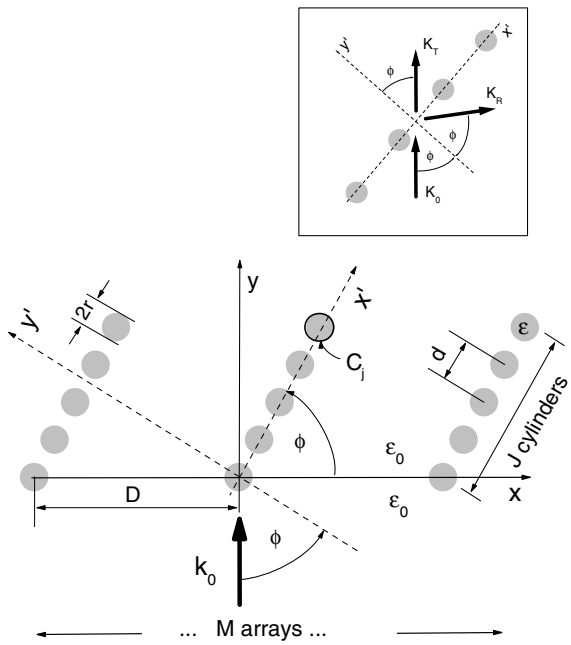


**Figure 1.** Configuration of the scattering problem: a linearly polarized Gaussian beam illuminates a compound grating comprising subarrays of circular cylinders. The cylinder axes of each subarray are contained in the same plane and the planes corresponding to different subarrays are parallel to each other, forming an angle $\phi$ with respect to the periodicity direction. In this case $N = 15$, $M = 3$ and $J = 5$. Inset: propagation directions of incident $\mathbf{k}_0$, transmitted $\mathbf{k}_T$ and reflected $\mathbf{k}_R$ wavevectors in the $x'y'$ reference frame.

of each subarray. The cylinder axes of each subarray are contained in the same plane and the planes corresponding to different subarrays are parallel to each other, forming an angle $\phi$ with respect to the periodicity direction ($\hat{x}$). The subarrays are distributed periodically, forming a finite grating with period $D$ (see figure 1). The system is normally illuminated by a Gaussian beam of wavelength $\lambda$ and half-width $W$.

### 2.1. Scalar approach

To get physical insight on the expected behavior, in this section we develop a simple model which accounts for the response observed, without using the rigorous method which is very complex and demands large computation times.

Since the cylinders and the period of each subarray ($d$) are subwavelength, we developed a very simple scalar model to anticipate the behavior of such structures. The basic idea of the model proposed here is that the response of the dual-period structure can be regarded as the product of the response of the periodic structure of period $D$ and that of each subarray of period $d$. This idea is based on the scalar model for diffraction gratings [36]. A similar model was derived for compound wire gratings made of slits [31], where an expression of the intensity at a given point p on a screen far from the dual-period slit structure was obtained:

$$I_p = I_0 \left(\frac{\sin M\alpha}{\sin\alpha}\right)^2 \left(\frac{\sin J\gamma}{\sin\gamma}\right)^2 \left(\frac{\sin\beta}{\beta}\right)^2 = I_0 I_M I_J \left(\frac{\sin\beta}{\beta}\right)^2, \quad (1)$$

where $\alpha = \frac{\pi D}{\lambda}(\sin\theta - \sin\theta_0)$, $\gamma = \frac{\pi d}{\lambda}(\sin\theta - \sin\theta_0)$ and $\beta = \frac{\pi a}{\lambda}(\sin\theta - \sin\theta_0)$, where $\theta$ and $\theta_0$ are the observation and incidence angles, $a$ is the width of each slit and $I_0$ is the incident intensity. The first, second and third factors on the right-hand side of equation (1) can be identified as the interference of the $M$ subarrays ($I_M$), the interference of the $J$ cylinders ($I_J$) in each period and the diffraction of each element, respectively. We adapted this simple model to deal with structures comprising inclined subarrays, as shown in figure 1. In this case, the $M$ term remains the same—since it accounts for the interference among different periods—but in the $J$ term $\gamma$ should be defined as

$$\gamma = \frac{\pi d}{\lambda}(\sin\theta' - \sin\theta'_0), \tag{2}$$

where $\theta'$ and $\theta'_0$ are the observation and incidence angles in the primed reference system (see figure 1). Referring all the angles to the unprimed system, for normal illumination we get

$$\gamma = \frac{\pi d}{\lambda}[\sin(\theta - \phi) - \sin\phi]. \tag{3}$$

For slits much smaller than the wavelength, the third term in equation (1) does not affect the response and then the $M$ and $J$ terms govern the behavior of the dual-period structure. The $M$ term determines the directions of the diffraction orders, which are given by

$$\sin\theta_m = \sin\theta_0 + m\frac{\lambda}{D}, \qquad m \in Z \tag{4}$$

and the $J$ term, which involves the angle $\phi$, provides the possibility of designing the dual-period array to send the maximum intensity in a given direction. In particular, if this direction coincides with that of a diffraction order, a significant enhancement can be obtained. In this case

$$\sin(\theta_m - \phi) = \sin\phi + p\frac{\lambda}{d} \qquad p \in Z. \tag{5}$$

The maximum intensity of the $J$ term is obtained for $p = 0$ and then the optimum value of $\phi$ is $\phi = \theta_m/2$.

In figure 2 we show an example of the reflected response given by the scalar model for a finite array comprising five subarrays of five cylinders each, and for the following parameters: $\lambda/d = 3$, $\lambda/D = 0.6$, $\phi = 18.43°$ ($M = J = 5$). The value of $\phi$ was chosen so as to maximize the intensity in the direction of the $+1$ order. It is evident from the curves that the $J$ term modulates the response given by the $M$ term, and thus the intensity of the $+1$ order ($\theta \approx 37°$) is maximized, whereas those of the $-1$ ($\theta \approx -37°$) and of the specular order ($\theta = 0°$) are almost canceled out. This constitutes a blazing effect obtained, in this case, by an array of subwavelength apertures distributed in the form of a dual-period grating. It is important to remark that this simple model considers perfectly conducting objects, disregarding the polarization of the incident wave and the thickness and geometry of the scattering elements.

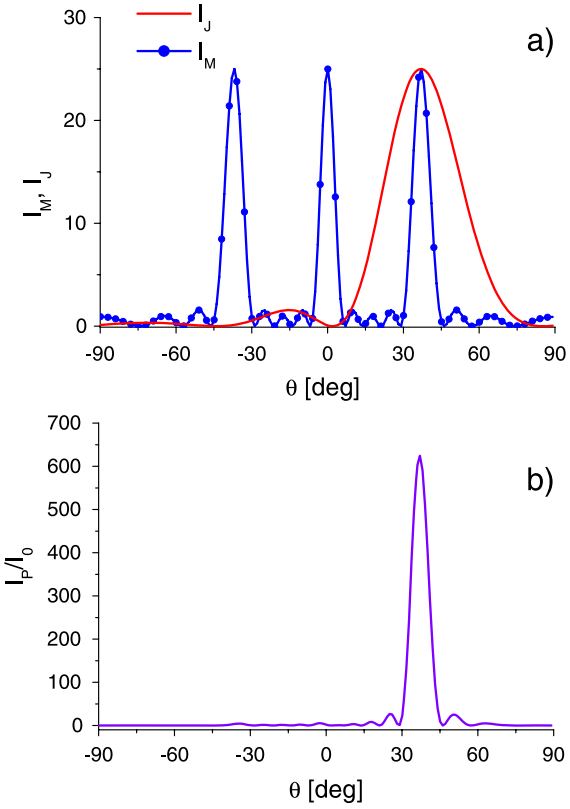


**Figure 2.** Reflected response of a finite array comprising five subarrays of five scatterers each, obtained by the scalar model, for $\lambda/d = 3$, $\lambda/D = 0.6$ and $\phi = 18.43°$ ($M = J = 5$). (a) $J$ term and $M$ term according to equation (1); (b) total reflected intensity.

### 2.2. Integral method

In what follows we summarize a general integral formalism based on the extinction theorem (ET) method applied to 2D systems, as is the case of the present study [32–35]. We consider an array of circular wires in vacuum (host medium). For systems with translation symmetry (2D geometries), the expressions for the scattered field in each medium are

$$\psi_\alpha^{(0)}(\mathbf{r}) = \psi_\alpha^{(\mathrm{inc})}(\mathbf{r}) + \sum_{j=1}^{N}\left\{\frac{\mathrm{i}}{4}\int_{C_j^{(+)}} \mathrm{d}l'\left[\frac{\partial H_0^{(1)}(\sqrt{\epsilon_0}k_0|\mathbf{r}-\mathbf{r}'|)}{\partial \mathbf{n}'}\right]\right.$$
$$\left.\times\,\psi_\alpha^{(0)}(\mathbf{r}') - H_0^{(1)}(\sqrt{\epsilon_0}k_0|\mathbf{r}-\mathbf{r}'|)\frac{\partial\psi_\alpha^{(0)}(\mathbf{r}')}{\partial\mathbf{n}'}\right\}, \tag{6}$$

$$\psi_\alpha^{(j)}(\mathbf{r}) = -\frac{\mathrm{i}}{4}\int_{C_j^{(-)}} \mathrm{d}l'\left[\frac{\partial H_0^{(1)}(\sqrt{\epsilon_1}k_0|\mathbf{r}-\mathbf{r}'|)}{\partial\mathbf{n}'}\psi_\alpha^{(j)}(\mathbf{r}')\right.$$
$$\left. - H_0^{(1)}(\sqrt{\epsilon_1}k_0|\mathbf{r}-\mathbf{r}'|)\frac{\partial\psi_\alpha^{(j)}(\mathbf{r}')}{\partial\mathbf{n}'}\right], \tag{7}$$

for $j = 1, \ldots, N$, where $\psi_\alpha^{(j)}(\mathbf{r})$ represents the complex amplitudes of the electric ($\alpha = s$) or the magnetic ($\alpha = p$) field in the host medium ($j = 0$), or within any of the $N$ scatterers ($j = 1, \ldots, N$); $\mathrm{d}l'$ is a differential element of a line over the contour $C_j$. The superscript $(+)$ in $C_j^{(+)}$ represents the cross-section contour of the $j$th scatterer when $\mathbf{r}'$ tends to $C_j$ from the host medium, and in this case $\mathbf{n}'$ points towards the interior of the $j$th medium. Conversely, $C_j^{(-)}$ represents

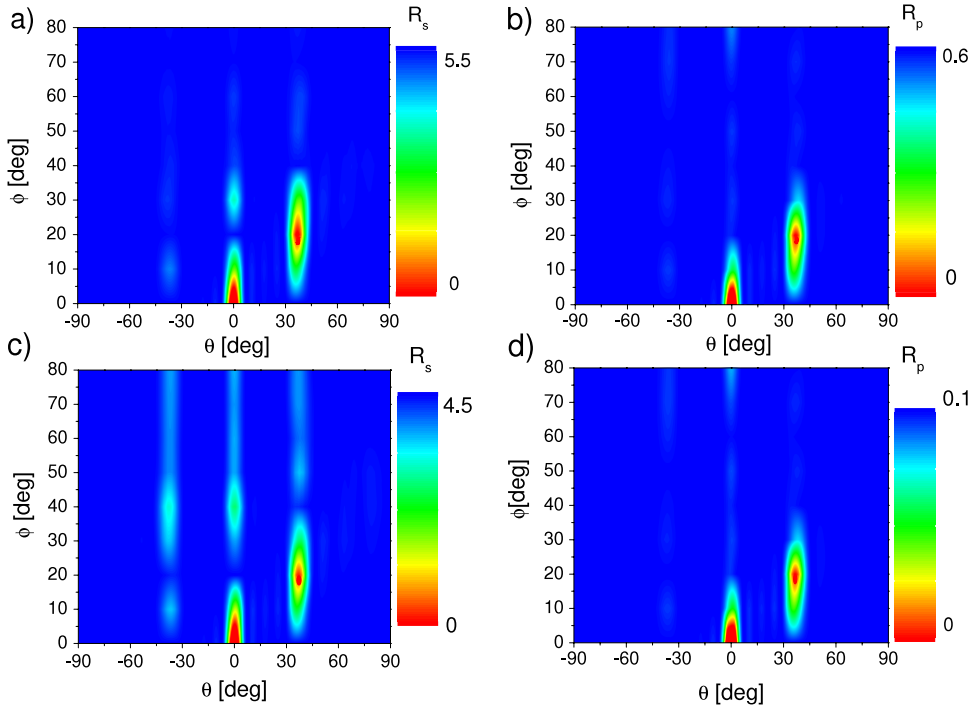


**Figure 3.** Contour plots of the reflection coefficient (equation (15)) as a function of the observation ($\theta$) and inclination ($\phi$) angles for an array formed by five subarrays, each of which comprises five cylinders of $r = 50$ nm, $\lambda = 800$ nm, $\lambda/D = 0.6$ ($D = 1333.33$ nm), $\lambda/d = 3$ ($d = 266.66$ nm). Panels (a) and (b) correspond to silver cylinders ($\epsilon_{\mathrm{Ag}} = -27.995 + \mathrm{i}1.523$) and panels (c) and (d) to silica cylinders ($\epsilon_{\mathrm{S}} = 3$). The vertical lines correspond to the specular and the $\pm 1$ reflected orders. (a) Silver cylinders, s polarization; (b) silver cylinders, p polarization; (c) silica cylinders, s polarization; (d) silica cylinders, p polarization.

the cross-section contour of the $j$th scatterer when $\mathbf{r}'$ tends to $C_j$ from the interior of the $j$th medium and $\mathbf{n}'$ points outwards of the $j$th medium. $H_0^{(1)}$ is the first-class zero-order Hankel function.

In 2D problems, the boundary conditions reduce to two separate equations for s and p modes:

$$[\psi_\alpha^{(0)}(\mathbf{r})]_{\mathbf{r}\in C_j^{(+)}} = [\psi_\alpha^{(j)}(\mathbf{r})]_{\mathbf{r}\in C_j^{(-)}}, \tag{8}$$

$$\left[\frac{\partial \psi_\alpha^{(0)}(\mathbf{r})}{\partial n'}\right]_{\mathbf{r}\in C_j^{(+)}} = \left[\eta_j(\alpha)\frac{\partial \psi_\alpha^{(j)}(\mathbf{r})}{\partial n'}\right]_{\mathbf{r}\in C_j^{(-)}}, \tag{9}$$

with $j = 1, 2, \ldots, N$ and $\eta_j(\mathrm{s}) = 1$, $\eta_j(\mathrm{p}) = \epsilon_1/\epsilon_0$ (we consider identical cylinders, $\epsilon_1 = \epsilon_2 = \cdots = \epsilon_j = \epsilon$). Equations (8) and (9) do not couple polarization modes, which implies that in a 2D system there is no cross-polarization.

To compute the far field, we make use of the asymptotic expression for the Hankel function when $|\mathbf{r} - \mathbf{r}'| \to \infty$, and substitute it in the previous equations:

$$\psi_\alpha^{(\mathrm{scatt})}(r, \theta_{\mathrm{r,t}}) = \frac{1}{4}\sqrt{\frac{2}{\pi(\epsilon_0)^{1/2}k_0 r}} \times \exp[\mathrm{i}(\sqrt{\epsilon_0}k_0 r - \pi/4)] \times A_\alpha^{\mathrm{r,t}}(\theta_{\mathrm{r,t}}), \tag{10}$$

where

$$A_\alpha^{\mathrm{r,t}}(\theta_{\mathrm{r,t}}) = \sum_{j=1}^{N}\left\{\int_{C_j^{(+)}} \mathrm{d}l'\left((\mathbf{n}'\cdot\mathbf{k}_{\mathrm{scatt}})\psi_\alpha^{(0)}(\mathbf{r}') - \mathrm{i}\frac{\partial \psi_\alpha^{(0)}(\mathbf{r}')}{\partial \mathbf{n}'}\right)\exp(-\mathrm{i}\mathbf{k}_{\mathrm{scatt}}\cdot\mathbf{r})\right\}, \tag{11}$$

where $\mathbf{k}_{\mathrm{scatt}}$ is the propagation vector, defined by

$$\mathbf{k}_{\mathrm{scatt}} = \sqrt{\epsilon_0}k_0(\sin\theta_{\mathrm{r,t}}, 0, \cos\theta_{\mathrm{r,t}}), \tag{12}$$

and $\theta_{\mathrm{r,t}}$ is the observation angle. Then, the reflected field corresponds to $-90° < \theta_{\mathrm{r}} \leqslant 90°$ and the transmitted field to $90° < \theta_{\mathrm{t}} \leqslant 270°$. The incident field appears in implicit form in the scattering equations.

To carry out the calculations we use an incident Gaussian beam defined as [37]

$$\psi_\alpha^{(\mathrm{inc})}(\mathbf{r}) = \exp[\mathrm{i}k_0(x\sin\theta_0 + y\cos\theta_0)g(x, y)] \times \exp[-(x\cos\theta_0 - y\sin\theta_0)^2/W^2], \tag{13}$$

where $\theta_0$ is the incidence angle, $W$ is the half-width at half-maximum and

$$g(x, y) = 1 + \frac{1}{\epsilon_0(k_0W)^2}\left[\frac{2}{W^2}(x\cos\theta_0 - y\sin\theta_0)^2 - 1\right]. \tag{14}$$

We define the angle-dependent reflection and transmission coefficients as

$$R_\alpha(\theta_{\mathrm{r}}) = \frac{|S_\alpha^{\mathrm{r}}|}{P_\alpha^{\mathrm{inc}}}$$
$$T_\alpha(\theta_{\mathrm{t}}) = \frac{|S_\alpha^{\mathrm{t}}|}{P_\alpha^{\mathrm{inc}}}, \tag{15}$$

where the incident power $P_\alpha^{\mathrm{inc}}$ is given by [37]

$$P_\alpha^{\mathrm{inc}} = \nu\frac{cW}{8\sqrt{2\pi}}\left[1 - \frac{1}{2(k_0W)^2}(1 + \tan^2\theta_0)\right] \tag{16}$$

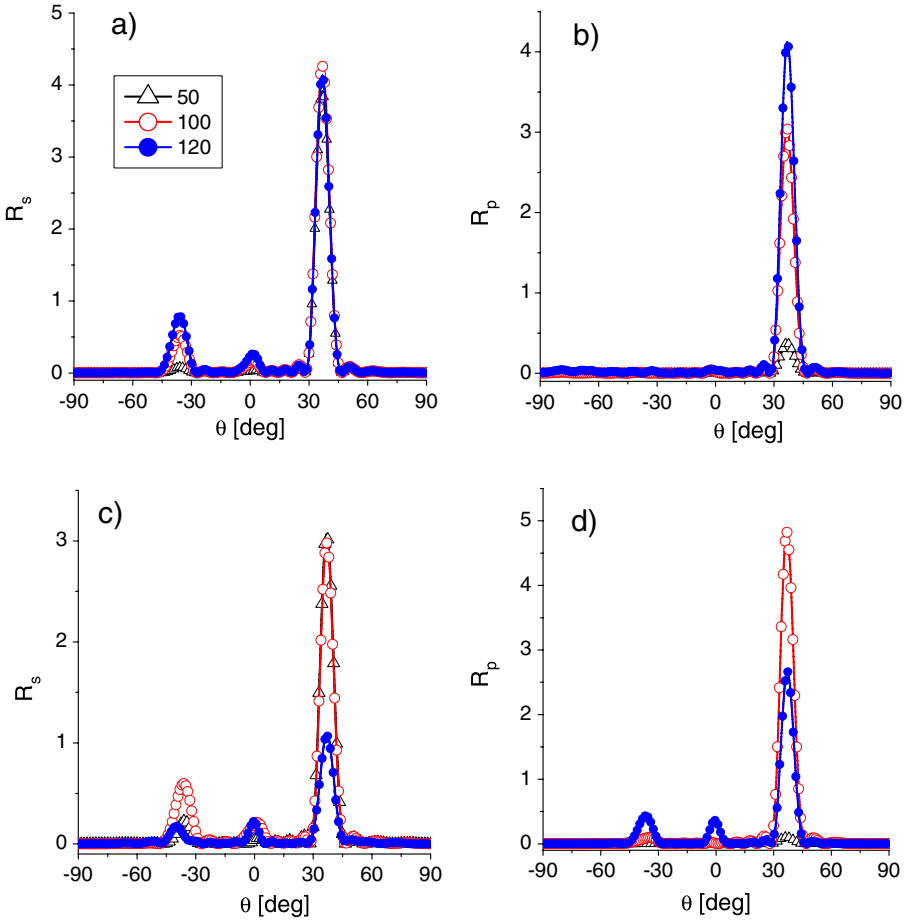


**Figure 4.** Reflection coefficient (equation (15)) as a function of the observation angle for an array comprising five subarrays of five cylinders, with $D = 1333.33$ nm, $d = 266.66$ nm, $\lambda = 800$ nm and $\phi = 18.43°$. Different curves correspond to different radii of the cylinders: $r = 50$ nm (triangles), $r = 100$ nm (hollow circles) and $r = 120$ nm (solid circles). (a) Silver cylinders, s polarization; (b) silver cylinders, p polarization; (c) silica cylinders, s polarization; (d) silica cylinders, p polarization.

$\nu = \sqrt{\epsilon_0}$ for s polarization and $\nu = 1/\sqrt{\epsilon_0}$ for p polarization, and $|S_\alpha^{\mathrm{r,t}}|$ is the absolute value of the Poynting vector for the reflected and the transmitted field (see equation (10)) and is given by

$$|S_\alpha^{\mathrm{r,t}}| = \frac{c}{16\pi^2 k_0}|A_\alpha^{\mathrm{r,t}}(\theta_{\mathrm{r,t}})|^2. \tag{17}$$

The total reflection $\rho_\alpha(\theta_0)$ and transmission $\tau_\alpha(\theta_0)$ coefficients can be obtained by

$$\rho_\alpha(\theta_0) = \int_{-90°}^{90°} R_\alpha(\theta_\mathrm{r})\,\mathrm{d}\theta_\mathrm{r} \tag{18}$$

$$\tau_\alpha(\theta_\mathrm{t}) = \int_{90°}^{270°} T_\alpha(\theta_\mathrm{t})\,\mathrm{d}\theta_\mathrm{t}. \tag{19}$$

In the following examples we have tested the numerical convergence of the integrals involved, and in all cases we obtained an error less than 0.01%. Energy conservation was achieved within an error of 0.001% in the case of dielectric cylinders, and of 0.02% in the case of silver cylinders when the imaginary part of the permittivity is neglected. For $\mathrm{Im}(\epsilon) \neq 0$ the sum of the reflected and the transmitted power is slightly smaller than the incident power due to absorption in the cylinders.

## 3. Numerical results

We implemented numerically the integral formalism (see section 2.2) to compute the field scattered (reflected and transmitted) by finite arrays of cylinders when illuminated by a Gaussian beam. In particular, we analyzed the response of dual-period arrays formed by metallic or dielectric cylinders with circular cross section in vacuum, distributed in several subarrays aligned in planes forming an angle $\phi$ with respect to the periodicity direction (see figure 1).

All the results shown correspond to structures with 25 cylinders in total ($N = 25$) distributed in five groups of five cylinders each ($M = J = 5$), illuminated by a normally incident Gaussian beam of width $W = 5000$ nm. Figure 3 shows contour plots of reflected intensity as a function of the observation angle $\theta$ and the inclination angle $\phi$. The radius of the cylinders is $r = 50$ nm, $\lambda = 800$ nm, $\lambda/D = 0.6$ ($D = 1333.33$ nm) and $\lambda/d = 3$ ($d = 266.66$ nm). In figures 3(a) and (b) the scatterers are silver cylinders (the dielectric constant of silver at $\lambda = 800$ nm is $\epsilon_{\mathrm{Ag}} = -27.995 + \mathrm{i}1.523$), and 3(c) and (d) correspond to silica cylinders ($\epsilon_{\mathrm{S}} = 3$). Figures 3(a) and (c) correspond to s polarization (electric field along the cylinder axes) and

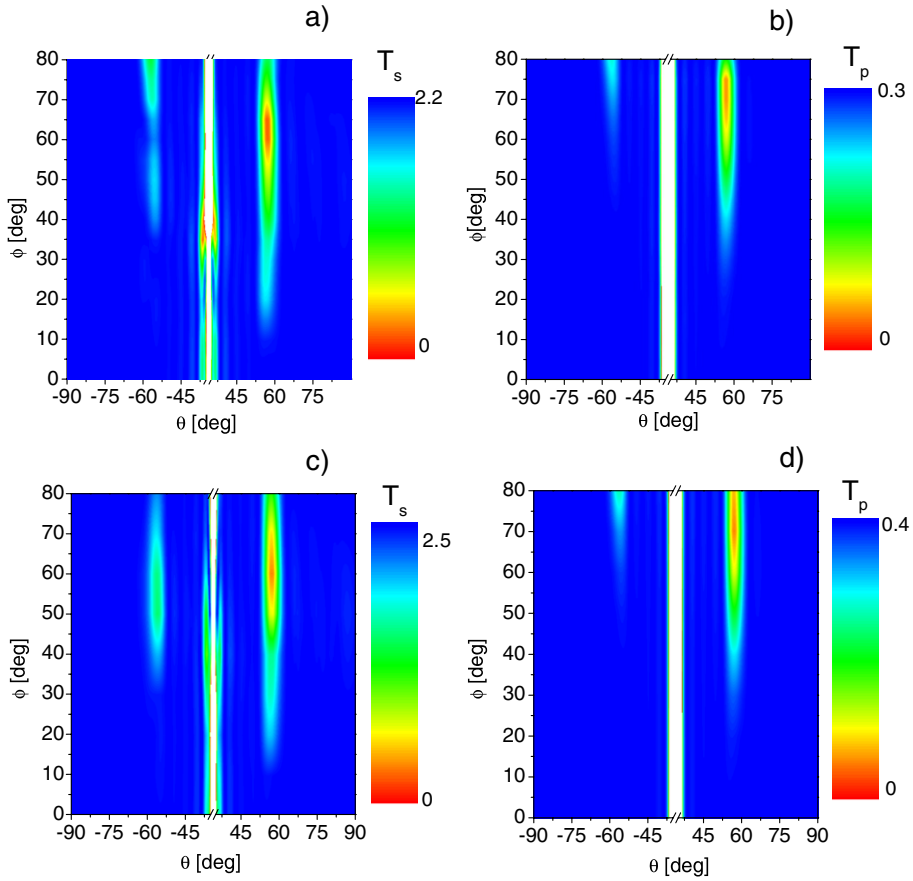


**Figure 5.** Contour plots of the transmission coefficient (equation (15)) as a function of the observation ($\theta$) and inclination ($\phi$) angles, for the same structure and incidence parameters of figure 3. (a) Silver cylinders, s polarization; (b) silver cylinders, p polarization; (c) silica cylinders, s polarization; (d) silica cylinders, p polarization.

figures 3(b) and (d) to p polarization (magnetic field along the cylinder axes). These intensity maps clearly show three vertical fringes at the observation angles corresponding to the specular and to the $\pm 1$ reflected orders. The $\theta$ location of these maxima are independent of $\phi$, since these directions—diffraction orders in the infinite grating case—are only determined by the wavelength and the period $D$ of the structure. In this case these angles are $\theta_{\pm} = 36.8°$. Although the inclination angle $\phi$ does not affect the maxima directions, it is evident from the curves that $\phi$ modifies the intensity distribution. For $\phi = 0$ the symmetry of the structure produces a symmetric power distribution, most of which propagates in the specular direction. As $\phi$ increases, more power propagates in the positive region of observation angles and, as predicted by the scalar model, the optimum angle at which the power carried by the $+1$ order is maximized is $\phi \approx 18.4°$. A further increase of $\phi$ reduces the power in the $+1$ order direction, as can be noticed in all the plots, for both polarization modes and for silver and silica cylinders. According to the scalar model described in section 2, the value of $\phi$ that optimizes the intensity in the $+1$ order direction for this configuration is $\phi \approx 18.4°$, and this estimation agrees very well with the results obtained by the rigorous calculation, as can be observed in figure 3. It is important to remark that the behavior observed is similar for metallic as well as for dielectric cylinders, and this confirms that the enhancement produced by this kind of compound structure is purely a geometric effect and does not depend on the material of the scatterers [32]. In both cases (silver and silica), the relative intensity in the $+1$ order direction is maximized. Notice that, even in the silica case, which is further than the silver case from the assumptions of the scalar model for the case of dielectric cylinders, the simple model predicts the optimum enhancement direction very accurately.

In order to confirm that the only responsible parameter for the blaze-like effect is the inclination angle $\phi$, we performed calculations of reflected intensity for different arrays varying only the radius of the cylinders and keeping the rest of the parameters fixed, with the same values as those in figure 3. These results are shown in figure 4 for silver cylinders (figures 4(a) and (b)) and for silica cylinders (figures 4(c) and (d)). All the curves correspond to $\phi = 18.43°$ which, according to the scalar model, maximizes the intensity in the $+1$ order direction. Even though the intensity in this direction depends on the radius of the cylinders, it is evident from all the curves that the relative intensity in this direction is maximized. The total intensity scattered by the arrays is different in each case, and this can be understood if we take into account that each subarray can be regarded as a slab with an effective dielectric permittivity which depends on the filling factor.

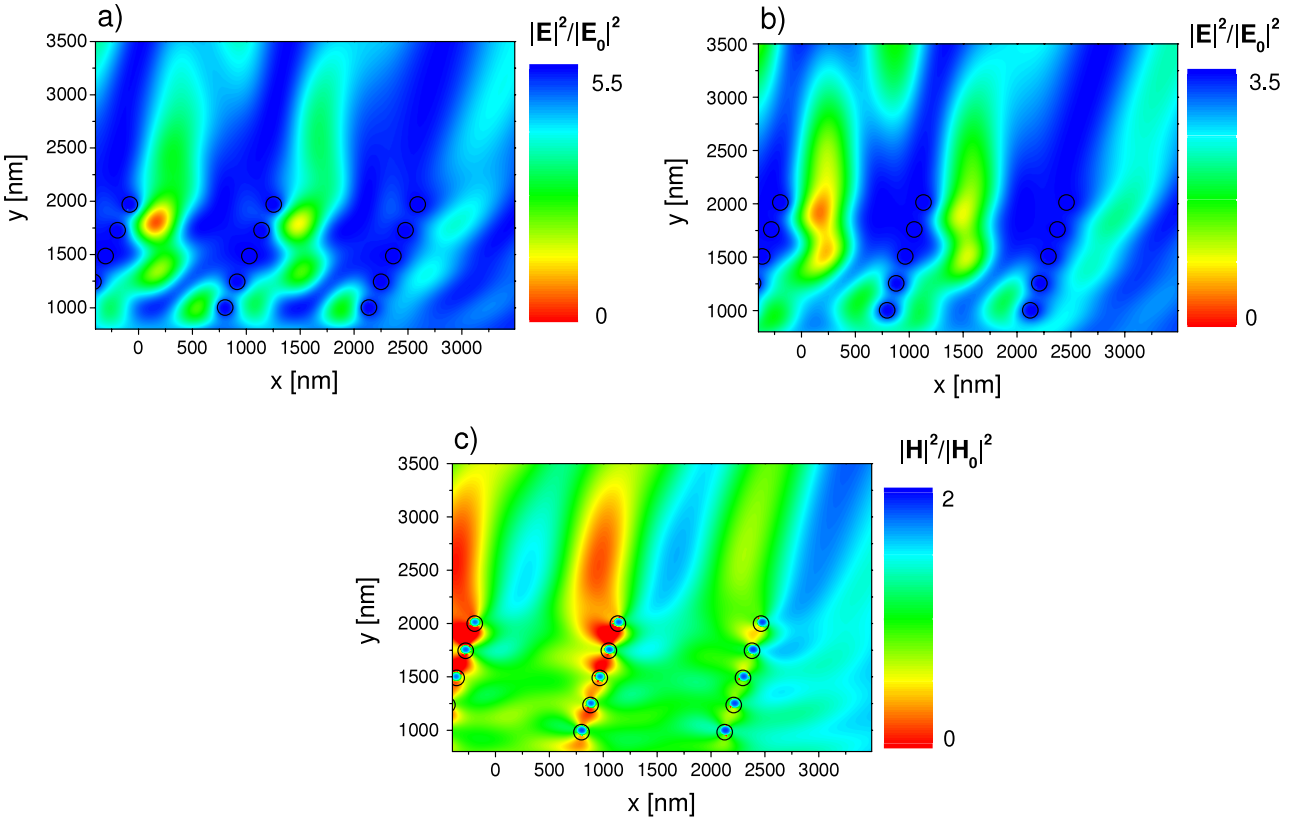


**Figure 6.** Near-field plots for the silver structure considered in figure 5 for different $\phi$ values. (a) s polarization and $\phi = 62.5°$; (b) s polarization and $\phi = 71.5°$; (c) p polarization and $\phi = 71.5°$.

Since the period $d$ of each subarray is fixed, the filling factor varies with the radius of the cylinders.

The intensity maps of figure 5 correspond to the transmission response of the same structures considered in figure 3 for both polarization modes, for silver cylinders (figures 5(a) and (b)) and for silica cylinders (figures 5(c) and (d)). The transmitted response presents intensity maxima located in the same $\theta$ directions of the reflected maxima, as predicted by the grating equation for a grating of period $D$ under normal illumination (4). However, in this case the inclination angles that maximize the intensity in the $+1$ transmitted order direction are $\phi \approx 62.5°$ for s polarization and $\phi \approx 71.5°$ for p polarization. For these large values of $\phi$ it is to be expected that resonant mechanisms such as cavity modes and coupling will be involved in the diffraction process. However, to get some physical insight into these results we apply a simple model again. If each subarray is regarded as a plane for the incident wave—we recall that the distance between adjacent cylinders is much smaller than the wavelength of the incident wave—an intensification of the transmitted beam should occur for the direction specularly reflected at this plane. For $\phi > 45°$ the beam specularly reflected by each plane propagates towards the $y > 0$ half-space (see the inset in figure 1), i.e. it becomes part of the transmitted field. According to the definition of the observation angle in the transmission case, the intensification direction is $\theta = \pi - 2\phi$. To enhance the $m$th order, this angle should be the same as that of the transmitted order given by the grating equation (4). Then the optimum $\phi$ value is given by

$$\phi = \frac{\pi - \arcsin(m\frac{\lambda}{D})}{2}. \tag{20}$$

For the parameters of figure 5 this estimation leads to $\phi = 71.5°$, which is in very good agreement with the maximum intensity shown in figures 5(b) and (d) for p polarization. However, for the s case the maximum is slightly shifted from this value. This shift can be attributed to the excitation of a cavity mode within the structure: since the diameter of the cylinders and the distance between them are subwavelength, each subarray can be regarded as a slab, with an effective dielectric constant. Therefore, an open cavity is formed between subarrays, whose length and width are approximately $l = D(1 - \cos\phi)$ and $w = D\sin\phi$, respectively. For $l/\lambda \approx 1$, a longitudinal mode is excited while the field within the cavity is intensified, producing an enhancement of the transmitted field in the allowed directions. For the parameters of figure 5 and for $\phi = 62.5°$, $l \simeq 0.9\lambda$ and $w \simeq 1.5\lambda$, establishing an eigenmode between subarrays, as can be observed in the near-field plot in figure 6(a). It is evident from figure 6(b) that the near field is still dominated by this mode for $\phi = 71.5°$, which inhibits the intensification of the transmitted $+1$ order by the specular effect described before. For this value of $\phi$ the picture is different for p polarization, where the main intensification mechanism is a significant coupling between neighboring cylinders of the same subarray, as can be observed in figure 6(c).

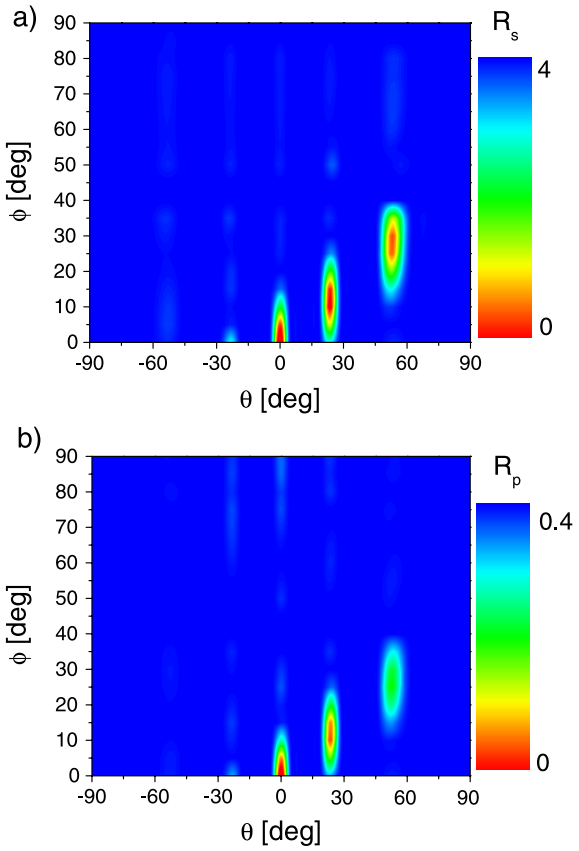


**Figure 7.** Contour plots of the reflection coefficient (equation (15)) as a function of the observation ($\theta$) and inclination ($\phi$) angles, for an array formed by five subarrays, each of which comprises five silver cylinders, $r = 50$ nm, $\lambda = 810$ nm, $\lambda/D = 0.4$ ($D = 2025$ nm), $\lambda/d = 3$ ($d = 270$ nm). The vertical lines correspond to the specular, $\pm 1$, and $\pm 2$ reflected orders. (a) s polarization; (b) p polarization.

Another example of the blazing property of dual-period arrays is shown in figure 7, for which $\lambda/D = 0.4$, and therefore the $\pm 2$ diffraction orders are also propagating. This system comprises five subarrays, each formed by five silver cylinders of radius $r = 50$ nm, $\lambda = 810$ nm, $d = 270$ nm and $D = 2025$ nm. We show contour plots of reflected intensity as a function of $\theta$ and $\phi$. The directions corresponding to the propagating orders are now $\theta_{\pm 1} = 23.5°$ and $\theta_{\pm 2} = 53.1°$. These directions can be clearly identified as vertical fringes in the maps corresponding to s (figure 7(a)) and p (figure 7(b)) polarization modes. It can be observed that the intensity reflected in each order strongly depends on the inclination angle, and that the maximum enhancement is obtained for the $\phi$ values predicted by the simple model presented in section 2, according to which the $+1$ and the $+2$ orders should be intensified for $\phi = 11.8°$ and $26.5°$.

These results show that, with dual-period arrays of subwavelength characteristics, a blazing effect can be obtained for the reflection as well as for the transmission. It should be noticed that this effect strongly depends only on the period $D$ and the inclination angle $\phi$, but it is independent of the cylinders' cross section and material, the incident polarization and the subarray period $d$, as long as it is subwavelength. These characteristics provide flexibility for the design of optical devices since the material and geometry of the scatterers can be chosen to simplify the manufacturing processes while keeping the properties of dual-period structures.

The enhancement properties of the dual-period arrays described above arise from a purely geometric effect and, as such, the structures can be rescaled to produce the same effects in other regions of the electromagnetic spectrum.

## 4. Concluding remarks

We investigated the blazing effect produced by dual-period arrays of cylinders formed by subarrays inclined with respect to the periodicity direction. The subwavelength characteristic of the scatterers and of the distance between them is a key factor to get the enhancement. Both polarization modes were analyzed. We considered metallic as well as dielectric cylinders and showed that the material is not a critical factor to obtain the effect. It was found that, with this kind of structure, a blazing effect can be obtained for reflection as well as for transmission. Even though the proposed structures involve subwavelength scatterers (nanowires in the optical range), optical devices with these characteristics can be fabricated with present-day technology. It was shown that for large inclination angles the scattering process involves several mechanisms that cannot be accounted for by the scalar model. Further investigation on the complex response of these systems is being carried out. It is important to remark that, although this study has been done in the optical range of the spectrum, no difficulties in the computer models are expected for larger structures working in a longer wavelengths regime. Moreover, the results show that the response of the dual-period structures is basically produced by its geometry, and therefore a similar behavior is expected for lower frequencies.

## Acknowledgments

The authors gratefully acknowledge partial support from Consejo Nacional de Investigaciones Científicas y Técnicas (CONICET), Universidad de Buenos Aires (UBA-X283, UBA-X150), Universidad Nacional de la Provincia de Buenos Aires (UNICEN) and Agencia Nacional de Promoción Científica y Tecnológica (ANPCYT-BID 802/OC-AR03-14099). This work was also supported by a grant of Red Argentina de Optica y Fotofísica.

## References

[1] Tan W-C, Sambles J R and Preist T W 2000 Double-period zero-order metal gratings as effective selective absorbers *Phys. Rev.* B **61** 13177–82

[2] Hibbins A and Sambles J R 2002 Excitation of remarkably nondispersive surface plasmons on a nondiffracting, dual-pitch metal grating *Appl. Phys. Lett.* **80** 2410–2

[3] Lockyear M J, Hibbins A P, Sambles J R and Lawrence C R 2005 Low angular-dispersion microwave absorption of a metal dual-period nondiffracting hexagonal grating *Appl. Phys. Lett.* **86** 184103

[4] Lepage J-F and McCarthy N 2004 Analysis of the diffractional properties of dual-period apodizing gratings: theoretical and experimental results *Appl. Opt.* **43** 3504–12

[5] Crouse D and Keshavareddy P 2006 A method for designing electromagnetic resonance enhanced silicon-on-insulator metal–semiconductor–metal photodetectors *J. Opt. A: Pure Appl. Opt.* **8** 175181
[6] Crouse D, Arend M, Zou J and Keshavareddy P 2006 Numerical modeling of electromagnetic resonance enhanced silicon metal–semiconductor–metal photodetectors *Opt. Express* **14** 2047–61
[7] Crouse D 2005 Numerical modeling and electromagnetic resonant modes in complex grating structures and optoelectronic device applications *IEEE Trans. Electron Devices* **52** 2365–73
[8] Wang Y, Chen Y, Zhang Y and Liu S 2007 Influence of grooves in the electromagnetic transmission of a periodic metallic grating filter *Opt. Commun.* **271** 132–6
[9] Fantino A N, Grosz S I and Skigin D C 2001 Resonant effect in periodic gratings comprising a finite number of grooves in each period *Phys. Rev.* E **64** 016605
[10] Grosz S I, Skigin D C and Fantino A N 2002 Resonant effects in compound diffraction gratings: influence of the geometrical parameters of the surface *Phys. Rev.* E **65** 056619
[11] Skigin D C, Fantino A N and Grosz S I 2003 Phase resonances in compound metallic gratings *J. Opt. A: Pure Appl. Opt.* **5** S129–35
[12] Depine R A, Fantino A N, Grosz S I and Skigin D C 2007 Phase resonances in obliquely illuminated compound gratings *Optik Int. J. Light Electron Opt.* **118** 42–52
[13] Le Perchec J, Barbara A, Quemerais P and López-Ríos T 2007 Role of commensurate arrangements in the optical response of metallic gratings arXiv:0706.3843
[14] Skigin D C and Depine R A 2005 Transmission resonances in metallic compound gratings with subwavelength slits *Phys. Rev. Lett.* **95** 217402
Paper selected for publication in the 2005 *Virtual J. Nanoscale Sci. Technol.* **12** (22)
[15] Skigin D C and Depine R A 2006 Resonances on metallic compound transmission gratings with subwavelength wires and slits *Opt. Commun.* **262** 270–5
[16] Skigin D C and Depine R A 2006 Narrow gaps for transmission through metallic structures gratings with subwavelength slits *Phys. Rev.* E **74** 046606
Paper selected for publication in the 2006 *Virtual J. Nanoscale Sci. Technol.* **14** (17)
[17] Hibbins A P, Hooper I R, Lockyear M J and Sambles J R 2006 Microwave transmission of a compound metal grating *Phys. Rev. Lett.* **96** 257402
[18] Skigin D C, Loui H, Popovic Z and Kuester E 2007 Bandwidth control of forbidden transmission gaps in compound structures with subwavelength slits *Phys. Rev.* E **76** 016604
[19] Sauvan C, Lalanne P and Lee M-Si L 2004 Broadband blazing with artificial dielectrics *Opt. Lett.* **29** 1593–5
[20] Ribot C, Lalanne P, Lee M-S-L, Loiseaux B and Huignard J-P 2007 Analysis of blazed diffractive optical elements formed with artificial dielectrics *J. Opt. Soc. Am.* A **24** 3819–26
[21] Haïdar R, Vincent G, Guérineau N, Collin S, Velghe S and Primot J 2005 Wollaston prism-like devices based on blazed dielectric subwavelength gratings *Opt. Express* **13** 9941–53
[22] Pajewski L, Borghi R, Schettini G, Frezza F and Santarsiero M 2001 Design of a binary grating with subwavelength features that acts as a polarizing beam splitter *Appl. Opt.* **40** 5898–05
[23] Astilean S, Lalanne P, Chavel P, Cambril E and Launois H 1998 High-efficiency subwavelength diffractive element patterned in a high-refractive-index material for 633 nm *Opt. Lett.* **23** 552–4
[24] Oonishi T, Konishi T and Itoh K 2007 Deterministic design of binary phase-only blazed grating with subwavelength features under limitation on spatial resolution of fabrication technique *Appl. Opt.* **46** 5019–26
[25] Kowalski M P, Heilmann R K, Schattenburg M L, Chang C-H, Berendse F B and Hunter W R 2006 Near-normal-incidence extreme-ultraviolet efficiency of a flat crystalline anisotropically etched blazed grating *Appl. Opt.* **45** 1676–9
[26] Osterried K, Heidemann K F and Nelles B 1998 Groove profile modification of blazed gratings by dip coating with hardenable liquids *Appl. Opt.* **37** 8002–7
[27] Jonsson J C and Nikolajeff F 2004 Optical properties of injection molded subwavelength gratings *Opt. Express* **12** 1924–31
[28] Kleemann B H, Ruoff J and Arnold R 2005 Area-coded effective medium structures, a new type of grating design *Opt. Lett.* **30** 1617–9
[29] Lalanne P, Astilean S, Chavel P, Cambril E and Launois H 1998 Blazed binary subwavelength gratings with efficiencies larger than those of conventional échelette gratings *Opt. Lett.* **23** 1081–3
[30] Lalanne P, Astilean S, Chavel P, Cambril E and Launois H 1999 Design and fabrication of blazed binary diffractive elements with sampling periods smaller than the structural cutoff *J. Opt. Soc. Am.* A **16** 1143–56
[31] Skigin D C and Depine R A 2007 Diffraction by dual-period gratings *Appl. Opt.* **46** 1385–91
[32] Lester M, Skigin D C and Depine R A 2008 Control of the diffracted response of wire arrays with double period *Appl. Opt.* **47** 1711–7
[33] Madrazo A and Nieto-Vesperinas M 1995 Scattering of electromagnetic waves from a cylinder in front of a conducting plane *J. Opt. Soc. Am.* A **12** 1298
[34] Scaffardi L B, Lester M, Skigin D C and Tocho J O 2007 Optical extinction spectroscopy used to characterize metallic nanowires *Nanotechnology* **18** 315402
[35] Lester M and Skigin D 2007 Coupling of evanescent s-polarized waves to the far field by waveguide modes in metallic arrays *J. Opt. A: Pure Appl. Opt.* **9** 81
[36] Born M and Wolf E 1999 *Principles of Optics* 7th edn (Cambridge: Cambridge University Press) pp 446–53
[37] Maradudin A A, Michel T, McGurn A and Méndez E 1990 Enhanced backscattering of light from a random grating *Ann. Phys.* **203** 244–207